SphereNet: Learning Spherical Representations for Detection and Classification in Omnidirectional Images

Benjamin Coors[1,3], Alexandru Paul Condurache[2,3], and Andreas Geiger[1]

[1] Autonomous Vision Group, MPI for Intelligent Systems and University of Tübingen
[2] Institute for Signal Processing, University of Lübeck
[3] Robert Bosch GmbH

Abstract. Omnidirectional cameras offer great benefits over classical cameras wherever a wide field of view is essential, such as in virtual reality applications or in autonomous robots. Unfortunately, standard convolutional neural networks are not well suited for this scenario as the natural projection surface is a sphere which cannot be unwrapped to a plane without introducing significant distortions, particularly in the polar regions. In this work, we present SphereNet, a novel deep learning framework which encodes invariance against such distortions explicitly into convolutional neural networks. Towards this goal, SphereNet adapts the sampling locations of the convolutional filters, effectively reversing distortions, and wraps the filters around the sphere. By building on regular convolutions, SphereNet enables the transfer of existing perspective convolutional neural network models to the omnidirectional case. We demonstrate the effectiveness of our method on the tasks of image classification and object detection, exploiting two newly created semi-synthetic and real-world omnidirectional datasets.

1 Introduction

Over the last years, omnidirectional imaging devices have gained in popularity due to their wide field of view and their widespread applications ranging from virtual reality to robotics [10,16,21,27,28]. Today, omnidirectional action cameras are available at an affordable price and 360° viewers are integrated into social media platforms. Given the growing amount of spherical imagery, there is an increasing interest in computer vision models which are optimized for this kind of data.

The most popular representation of 360° images is the equirectangular projection where latitude and longitude of the spherical image are mapped to horizontal and vertical grid coordinates, see Figs. 1+2 for an illustration. However, the equirectangular image representation suffers from heavy distortions in the polar regions which implies that an object will appear differently depending on its latitudinal position. This presents a challenge to modern computer vision algorithms, such as convolutional neural networks (CNNs) which are the state-of-the-art solution to many computer vision tasks.

While CNNs are capable of learning invariances to common object transformations and intra-class variations, they would require significantly more parameters, training samples and training time to learn invariance to these distortions from data. This is undesirable as data annotation is time-consuming and annotated omnidirectional datasets

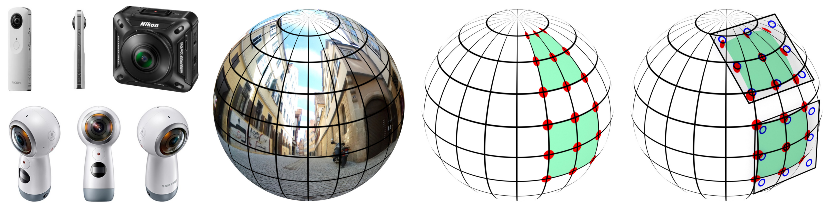

(a) 360° Cameras (b) 360° Image (c) Regular Kernel (d) SphereNet Kernel

Fig. 1: **Overview.** (a+b) Capturing images with fisheye or 360° action camera results in images which are best represented on the sphere. (c) Using regular convolutions (e.g., with 3×3 filter kernels) on the rectified equirectangular representation (see Fig. 2b) suffers from distortions of the sampling locations (red) close to the poles. (d) In contrast, our SphereNet kernel exploits projections (red) of the sampling pattern on the tangent plane (blue), yielding filter outputs which are invariant to latitudinal rotations.

are scarce and smaller in size than those collected for the perspective case. An attractive alternative is therefore to encode invariance to geometric transformations directly into a CNN, which has been proven highly efficient in reducing the number of model parameters as well as the required number of training samples [4, 29].

In this work, we present *SphereNet*, a novel framework for processing omnidirectional images with convolutional neural networks by encoding distortion invariance into the architecture of CNNs. SphereNet adjusts the sampling grid locations of the convolutional filters based on the geometry of the spherical image representation, thus avoiding distortions as illustrated in Figs. 1+2. The SphereNet framework applies to a large number of projection models including perspective, wide-angle, fisheye and omnidirectional projection. As SphereNet builds on regular convolutional filters, it naturally enables the transfer of CNNs between different image representations by adapting the sampling locations of the convolution kernels. We demonstrate this by training object detectors on perspective images and transferring them to omnidirectional inputs. We provide extensive experiments on semi-synthetic as well as real-world datasets which demonstrate the effectiveness of the proposed approach for image classification and object detection. In summary, this paper makes the following **contributions**:

- We introduce SphereNet, a framework for learning spherical image representations by encoding distortion invariance into convolutional filters. SphereNet retains the original spherical image connectivity and, by building on regular convolutions, enables the transfer of perspective CNN models to omnidirectional inputs.
- We improve the computational efficiency of SphereNet using an approximately uniform sampling of the sphere which avoids oversampling in the polar regions.
- We create two novel semi-synthetic and real-world datasets for object detection in omnidirectional images.
- We demonstrate improved performance as well as SphereNet's transfer learning capabilities on the tasks of image classification and object detection and compare our results to several state-of-the-art baselines.

2 Related Work

There are few deep neural network architectures specifically designed to operate on omnidirectional inputs. In this section, we review the most related approaches.

Khasanova et al. [14] propose a graph-based approach for omnidirectional image classification. They represent equirectangular images using a weighted graph, where each image pixel is a vertex and the weights are designed to minimize the difference between filter responses at different image locations. This graph structure is processed by a graph convolutional network, which is invariant to rotations and translations [15]. While a graph representation solves the problem of discontinuities at the borders of an equirectangular image, graph convolutional networks are limited to small graphs and image resolutions (50×50 pixels in [15]) and have not yet demonstrated recognition performance comparable to regular CNNs on more challenging datasets. In contrast, our method builds on regular convolutions, which offer state-of-the-art performance for many computer vision tasks, while also retaining the spherical image connectivity.

In concurrent work, Cohen et al. [3] propose to use spherical CNNs for classification and encode rotation equivariance into the network. However, often full rotation invariance is not desirable: similar to regular images, 360° images are mostly captured in one dominant orientation (i.e., it is rare that the camera is flipped upside-down). Incorporating full rotation invariance in such scenarios reduces discriminative power as evidenced by our experiments. Furthermore, unlike our work which builds on regular convolutions and is compatible with modern CNN architectures, it is non-trivial to integrate either graph or spherical convolutions into network architectures for more complex computer vision tasks like object detection. In fact, no results beyond image classification are provided in the literature. In contrast, our framework readily allows for adapting existing CNN architectures for object detection or other higher-level vision tasks to the omnidirectional case. While currently only few large omnidirectional datasets exist, there are many trained perspective CNN models available, which our method enables to transfer to any omnidirectional vision task.

Su et al. [30] propose to process equirectangular images with regular convolutions by increasing the kernel size towards the polar regions. However, this adaptation of the convolutional filters is a simplistic approximation of distortions in the equirectangular representation and implies that weights can only be shared along each row, resulting in a significant increase in model parameters. Thus, this model is hard to train from scratch and kernel-wise pre-training against a trained perspective model is required. In contrast, we retain weight sharing across all rows and columns so that our model can be trained directly end-to-end. At the same time, our method better approximates the distortions in equirectangular images and allows for perspective-to-omnidirectional representation transfer.

One way of mitigating the problem of learning spherical representations are cube map projections as considered in [19, 22]. Here, the image is mapped to the six faces of a cube which are considered as image planes of six virtual perspective cameras and processed with a regular CNN. However, this approach does not remove distortions but only minimizes their effect. Besides, additional discontinuities at the patch boundaries are introduced and post-processing may be required to combine the individual outputs of each patch. We avoid these problems by providing a suitable representation for spherical signals which can be directly trained end-to-end.

Besides works on distortion invariance, several works focus on invariances to geometric transformations such as rotations or flips. Jaderberg et al. [11], introduce a separate network which learns to predict the parameters of a spatial transformation of an input feature map. Scattering convolution networks [1,25] use predefined wavelet filters to encode stable geometric invariants into networks while other recent works encode invariances into learned convolutional filters [4, 9, 29, 31]. These works are orthogonal to the presented framework and can be advantageously combined.

Several recent works also consider adapting the sampling locations of convolutional networks, either dynamically [5] or statically [12, 18]. Unlike our work, these methods need to learn the sampling locations during training, which requires additional model parameters and training steps. In contrast, we take advantage of the geometric properties of the camera to inject this knowledge explicitly into the network architecture.

3 Method

This section introduces the proposed SphereNet framework. First, we describe the adaptation of the sampling pattern to achieve distortion invariance on the surface of the sphere (Section 3.1). Second, we propose an approximation which uniformly samples the sphere to improve the computational efficiency of our method (Section 3.2). Finally, we present details on how to incorporate SphereNet into a classification model (Section 3.3) as well as how to perform object detection on spherical inputs (Section 3.4).

3.1 Kernel Sampling Pattern

The central idea of SphereNet is to lift local CNN operations (e.g. convolution, pooling) from the regular image domain to the sphere surface where fisheye or omnidirectional images can be represented without distortions. This is achieved by representing the kernel as a small patch tangent to the sphere as illustrated in Fig. 1d. Our model focuses on distortion invariance and not rotation invariance, as in practice $360°$ images are mostly captured in one dominant orientation. Thus, we consider upright patches which are aligned with the great circles of the sphere.

More formally, let S be the unit sphere with S^2 its surface. Every point $\mathbf{s} = (\phi, \theta) \in S^2$ is uniquely defined by its latitude $\phi \in [-\frac{\pi}{2}, \frac{\pi}{2}]$ and longitude $\theta \in [-\pi, \pi]$. Let further Π denote the tangent plane located at $\mathbf{s}_\Pi = (\phi_\Pi, \theta_\Pi)$. We denote a point on Π by its coordinates $\mathbf{x} \in \mathbb{R}^2$. The local coordinate system of Π is hereby centered at $\mathbf{s}$ and oriented upright. Let Π_0 denote the tangent plane located at $\mathbf{s} = (0, 0)$. A point $\mathbf{s}$ on the sphere is related to its tangent plane coordinates $\mathbf{x}$ via a gnomonic projection [20].

While the proposed approach is compatible with convolutions of all sizes, in the following we consider a 3×3 kernel, which is most common in state-of-the-art architectures [8, 26]. We assume that the input image is provided in equirectangular format which is the de facto standard representation for omnidirectional cameras of all form factors (e.g. catadioptric, dioptric or polydioptric). In Section 3.2 we consider a more efficient representation that improves the computational efficiency of our method.

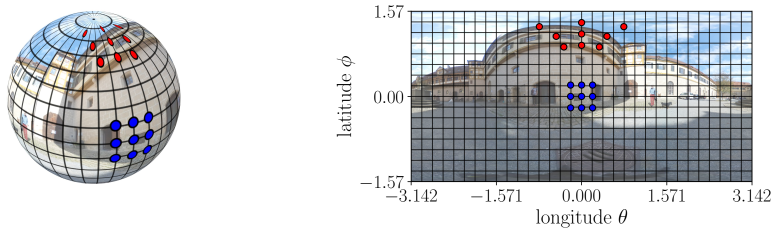

(a) Sphere (b) Equirectangular

Fig. 2: **Kernel Sampling Pattern** at $\phi = 0$ (blue) and $\phi = 1.2$ (red) in spherical (a) and equirectangular (b) representation. Note the distortion of the kernel at $\phi = 1.2$ in (b).

The kernel shape is defined so that its sampling locations $\mathbf{s}_{(j,k)}$, with $j, k \in \{-1, 0, 1\}$ for a 3×3 kernel, align with the step sizes Δ_θ and Δ_ϕ of the equirectangular image at the equator. This ensures that the image can be sampled at Π_0 without interpolation:

$$
\begin{aligned}
\mathbf{s}_{(0,0)} &= (0, 0) & (1)\\
\mathbf{s}_{(\pm 1,0)} &= (\pm\Delta_\phi, 0) & (2)\\
\mathbf{s}_{(0,\pm 1)} &= (0, \pm\Delta_\theta) & (3)\\
\mathbf{s}_{(\pm 1,\pm 1)} &= (\pm\Delta_\phi, \pm\Delta_\theta) & (4)
\end{aligned}
$$

The position of these filter locations on the tangent plane Π_0 can be calculated via the gnomonic projection [20]:

$$
\begin{aligned}
x(\phi, \theta) &= \frac{\cos\phi \sin(\theta - \theta_{\Pi_0})}{\sin\phi_{\Pi_0} \sin\phi + \cos\phi_{\Pi_0} \cos\phi \cos(\theta - \theta_{\Pi_0})} & (5)\\
y(\phi, \theta) &= \frac{\cos\phi_{\Pi_0} \sin\phi - \sin\phi_{\Pi_0} \cos\phi \cos(\theta - \theta_{\Pi_0})}{\sin\phi_{\Pi_0} \sin\phi + \cos\phi_{\Pi_0} \cos\phi \cos(\theta - \theta_{\Pi_0})} & (6)
\end{aligned}
$$

For the sampling pattern $\mathbf{s}_{(j,k)}$, this yields the following kernel pattern $\mathbf{x}_{(j,k)}$ on Π_0:

$$
\begin{aligned}
\mathbf{x}_{(0,0)} &= (0, 0) & (7)\\
\mathbf{x}_{(\pm 1,0)} &= (\pm\tan\Delta_\theta, 0) & (8)\\
\mathbf{x}_{(0,\pm 1)} &= (0, \pm\tan\Delta_\phi) & (9)\\
\mathbf{x}_{(\pm 1,\pm 1)} &= (\pm\tan\Delta_\theta, \pm\sec\Delta_\theta \tan\Delta_\phi) & (10)
\end{aligned}
$$

We keep the kernel shape on the tangent fixed. When applying the filter at a different location $\mathbf{s}_\Pi = (\phi_\Pi, \theta_\Pi)$ of the sphere, the inverse gnomonic projection is applied

$$
\begin{aligned}
\phi(x, y) &= \sin^{-1}\left(\cos\nu \sin\phi_\Pi + \frac{y \sin\nu \cos\phi_\Pi}{\rho}\right) & (11)\\
\theta(x, y) &= \theta_\Pi + \tan^{-1}\left(\frac{x \sin\nu}{\rho \cos\phi_\Pi \cos\nu - y \sin\phi_\Pi \sin\nu}\right)
\end{aligned}
$$

where $\rho = \sqrt{x^2 + y^2}$ and $\nu = \tan^{-1}\rho$.

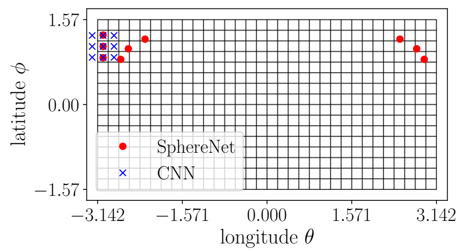

(a) Left Boundary

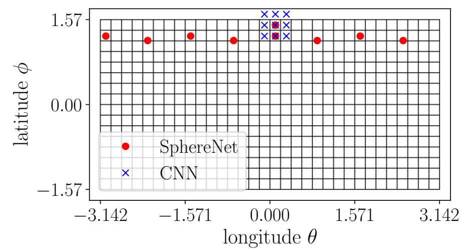

(b) Top Boundary

Fig. 3: **Sampling Locations.** This figure compares the sampling locations of SphereNet (red) to the sampling locations of a regular CNN (blue) at the boundaries of the equirectangular image. Note how the SphereNet kernel automatically wraps at the left image boundary (a) while correctly representing the discontinuities and distortions at the pole (b). SphereNet thereby retains the original spherical image connectivity which is discarded in a regular convolutional neural network that utilizes zero-padding along the image boundaries.

The sampling grid locations of the convolutional kernels thus get distorted in the same way as objects on a tangent plane of the sphere get distorted when projected from different elevations to an equirectangular image representation. Fig. 2 demonstrates this concept by visualizing the sampling pattern at two different elevations ϕ.

Besides encoding distortion invariance into the filters of convolutional neural networks, SphereNet additionally enables the network to wrap its sampling locations around the sphere. As SphereNet uses custom sampling locations for sampling inputs or intermediary feature maps, it is straightforward to allow a filter to sample data across the image boundary. This eliminates any discontinuities which are present when processing omnidirectional images with a regular convolutional neural network and improves recognition of objects which are split at the sides of an equirectangular image representation or which are positioned very close to the poles, see Fig. 3.

By changing the sampling locations of the convolutional kernels while keeping their size unchanged, our model additionally enables the transfer of CNN models between different image representations. In our experimental evaluation, we demonstrate how an object detector trained on perspective images can be successfully applied to the omnidirectional case. Note that our method can be used for adapting almost any existing deep learning architecture from perspective images to the omnidirectional setup. In general, our SphereNet framework can be applied as long as the image can be mapped to the unit sphere. This is true for many imaging models, ranging from perspective over fisheye[4] to omnidirectional models. Thus, SphereNet can be seen as a generalization of regular CNNs which encodes the camera geometry into the network architecture.

Implementation: As the sampling locations are fixed according to the geometry of the spherical image representation, they can be precomputed for each kernel location at

[4] While in some cases the single viewpoint assumption is violated, the deviations are often small in practice and can be neglected at larger distances.

every layer of the network. Further, their relative positioning is constant in each image row. Therefore, it is sufficient to calculate and store the sampling locations once per row and then translate them. We store the sampling locations in look-up tables. These look-up tables are used in a customized convolution operation which is based on highly optimized general matrix multiply (GEMM) functions [13]. As the sampling locations are real-valued, interpolation of the input feature maps is required. In our experiments, we compare nearest neighbor interpolation to bilinear interpolation. For an arbitrary sampling location (p_x, p_y) in a feature map f, interpolation is defined as:

$$\boxed{f(p_x, p_y) = \sum_{n}^{H} \sum_{m}^{W} f(m, n) g(p_x, m) g(p_y, n)} \tag{12}$$

with a bilinear interpolation kernel:

$$g(a, b) = max(0, 1 - |a - b|) \tag{13}$$

or a nearest neighbor kernel :

$$g(a, b) = \delta(\lfloor a + 0.5 \rfloor - b) \tag{14}$$

where $\delta(\cdot)$ is the Kronecker delta function.

3.2 Uniform Sphere Sampling

In order to improve the computational efficiency of our method, we investigate a more efficient sampling of the spherical image. The equirectangular representation oversamples the spherical image in the polar regions (see Fig. 4a), which results in near duplicate image processing operations in this area. We can avoid unnecessary computation in the polar regions by applying our method to a representation where data is stored uniformly on the sphere, in contrast to considering the pixels of the equirectangular image.

To sample points evenly from a sphere, we leverage the method of Saff and Kuijlaars [24] as it is fast to compute and works with an arbitrary number of sampling points N, including large values of N. More specifically, we obtain points along a spiral that encircles the sphere in a way that the distance between adjacent points along the spiral is approximately equal to the distance between successive coils of the spiral. As visualized in Fig. 4 for an equirectangular image with $N_e = 20 \times 10 = 200$ sampling points, this results in a sampling grid of $N = 127$ points with a similar sampling density to the equirectangular representation at the equator, while significantly reducing the number of sampling points at the poles.

To minimize the loss of information when sampling the equirectangular image we use bilinear interpolation. Afterwards, the image is represented by an $N \times c$ matrix, where c is the number of image channels. Unlike the equirectangular format, this representation no longer encodes the spatial position of each data point. Thus, we save this information in a separate matrix. This location matrix is used to compute the look-up tables for the kernel sampling locations as described in Section 3.1. Downsampling of the image is implemented by recalculating a reduced set of sampling points. For applying the kernels and downsampling the image nearest neighbor interpolation is used.

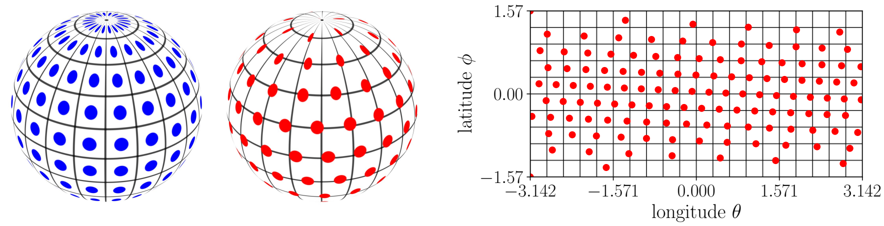

(a) Equirectangular Sphere Sampling

(b) Uniform Sphere Sampling
.

(c) Uniform Sampling in the Image Plane

Fig. 4: **Uniform Sphere Sampling.** Comparison of an equirectangular sampling grid on the sphere with $N = 200$ points (a) to an approximation of evenly distributing $N = 127$ sampling points on a sphere with the method of Saff and Kuijlaars [24] (b, c). Note that the sampling points at the poles are much more evenly spaced in the uniform sphere sampling (b) compared to the equirectangular representation (a) which oversamples the image in these regions.

3.3 Spherical Image Classification

SphereNet can be integrated into a convolutional neural network for image classification by adapting the sampling locations of the convolution and pooling kernels as described in Section 3.1. Furthermore, it is straightforward to additionally utilize a uniform sphere sampling (see Section 3.2), which we will compare to nearest neighbor and bilinear interpolation on an equirectangular representation in the experiments. The integration of SphereNet into an image classification network does not introduce novel model parameters and no changes to the training of the network are required.

3.4 Spherical Object Detection

In order to perform object detection on the sphere, we propose the *Spherical Single Shot MultiBox Detector (Sphere-SSD)*, which adapts the popular Single Shot MultiBox Detector (SSD) [17] to objects located on tangent planes of a sphere. SSD exploits a fully convolutional architecture, predicting category scores and box offsets for a set of default anchor boxes of different scales and aspect ratios. We refer the reader to [17] for details. As in the regular SSD, Sphere-SSD uses a weighted sum between a localization loss and confidence loss. However, in contrast to the original SSD, anchor boxes are now placed on tangent planes of the sphere and are defined in terms of spherical coordinates of their respective tangent plane, the width/height of the box on the tangent plane as well as an in-plane rotation. An illustration of anchor boxes at different scales and aspect ratios is provided in Fig. 5.

In order to match anchor boxes to ground truth detections, we select the anchor box closest to each ground truth box. During inference, we perform non-maximum suppression. For evaluation, we use the Jaccard index computed as the overlap of two polygonal regions which are constructed from the gnomonic projections of evenly spaced points along the rectangular bounding box on the tangent plane.

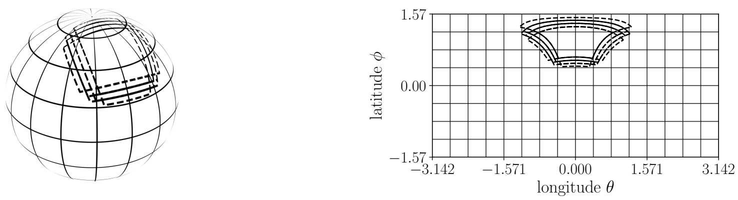

(a) Sphere (b) Equirectangular

Fig. 5: **Spherical Anchor Boxes** are gnomonic projections of 2D bounding boxes of various scales, aspect ratios and orientations on tangent planes of the sphere. The above figure visualizes anchors of the same orientation at different scales and aspect ratios on a 16×8 feature map on a sphere (a) and an equirectangular grid (b).

4 Experimental Evaluation

While the main focus of this paper is on the detection task, we first validate our model with respect to several existing state-of-the-art methods using a simple omnidirectional MNIST classification task.

4.1 Classification: Omni-MNIST

For the classification task, we create an omnidirectional MNIST dataset (*Omni-MNIST*), where MNIST digits are placed on tangent planes of the image sphere and an equirectangular image of the scene is rendered at a resolution of 60×60 pixels.

We compare the performance of our method to several baselines. First, we trained a regular convolutional network operating on the equirectangular images (EquirectCNN) as well as one operating on a cube map representation of the input (CubeMapCNN). We further improved the EquirectCNN model by combining it with a Spherical Transformer Network (SphereTN) which learns to undistort parts of the image by performing a global rotation of the sphere. A more in-depth description of the Spherical Transformer Network is provided in the supplemental. Finally, we also trained the graph convolutional network of Khasanova et al. [14] and the spherical convolutional model of Cohen et al. [3]. For [3] we use the code published by the authors[5]. As [14] does not provide code, we reimplemented their model based on the code of Defferrard et al. [6][6].

The network architecture for all models consist of two blocks of convolution and max-pooling, followed by a fully-connected layer. We use 32 filters in the first and 64 filters in the second layer and each layer is followed by a ReLU activation. The fully connected layer has 10 output neurons and uses a softmax activation function. In the CNN and SphereNet models, the convolutional filter kernels are of size 5×5 and are applied with stride 1. Max pooling is performed with kernels of size 3×3 and a stride of 2. The Spherical Transformer Network uses an identical network architecture but replaces the fully-connected output layer with a convolutional layer that outputs the

[5] https://github.com/jonas-koehler/s2cnn
[6] https://github.com/mdeff/cnn_graph

Table 1: **Classification Results on Omni-MNIST.** Performance comparison on the omnidirectional MNIST dataset.

Method	Test error (%)	# of Parameters
GCNN [14]	17.21	282K
S2CNN [3]	11.86	149K
CubeMapCNN	10.03	167K
EquirectCNN	9.61	196K
EquirectCNN+SphereTN	8.22	291K
SphereNet (Uniform)	7.16	144K
SphereNet (NN)	7.03	196K
SphereNet (BI)	**5.59**	196K

parameters of the rotation. After applying the predicted transformation of the Spherical Transformer the transformed output is then used as input to the EquirectCNN model.

Similarly, the graph convolutional baseline (GCNN) uses graph-conv layers with 32 and 64 filters of polynomial order 25 each, while the spherical CNN baseline (S2CNN) uses an S^2-conv layer with 32 filters and a $SO(3)$-conv layer with 64 filters. Downsampling in the S2CNN model is implemented with bandwidths of $30, 10, 6$ as suggested in [3]. Thus, all models have a comparable number of trainable model parameters (see Table 1). In addition, all models are trained with identical training parameters using Adam, a base learning rate of 0.0001 and batches of size 100 for 100 epochs.

Results on Omni-MNIST: Table 1 compares the performance of SphereNet with uniform sphere sampling (Uniform), nearest neighbor interpolation in the equirectangular image (NN) and bilinear interpolation in the equirectangular image (BI) to the baseline methods. Our results show that all three variants of SphereNet outperform all baselines.

Despite its high number of model parameters, the graph convolutional (GCNN) model struggles to solve the Omni-MNIST classification task. The spherical convolutional (S2CNN) model performs better but is outperformed by all CNN-based models. For the CNN-based models, the CubeMapCNN has a higher test error than EquirectCNN, most likely du to the discontinuities at cube borders and varying digit orientation in the top and bottom faces. The performance of the EquirectCNN is improved when combined with a Spherical Transformer Network (EquirectCNN+SphereTN), demonstrating that the SphereTN is able to support the classification task. However, it does not reach the performance of SphereNet, thus confirming the effectiveness of encoding distortion invariance into the network architecture itself compared to learning it from data.

For SphereNet, the uniform sphere sampling (Uniform) variant performs similar to the nearest neighbor (NN) variant, which demonstrates that the loss of information by uniformly sampling the sphere is negligible. SphereNet with bilinear interpolation (BI) overall performs best, improving upon all baselines by a significant margin.

Please consult the supplemental for further analysis on the impact of varying object scale, object elevation and choice of interpolation on the performance of each model.

Fig. 6: **Detection Results on FlyingCars Dataset.** The ground truth is shown in green, our SphereNet (NN) results in red.

Table 2: **Detection Results on FlyingCars Dataset.** All models are trained and tested on the FlyingCars dataset.

Method	Test mAP (%)	Training speed	Inference Speed
EquirectCNN+SphereTN	38.91	3.0 sec/step	0.232 sec/step
EquirectCNN	41.57	1.7 sec/step	0.091 sec/step
EquirectCNN++	45.65	3.1 sec/step	0.175 sec/step
CubeMapCNN	48.42	1.8 sec/step	0.095 sec/step
SphereNet (NN)	**50.18**	2.1 sec/step	0.101 sec/step

4.2 Object Detection: FlyingCars

We now consider the object detection task. Due to a lack of suitable existing omnidirectional image benchmarks, we create the novel *FlyingCars* dataset. FlyingCars combines real-world background images of an omnidirectional $360°$ action camera with rendered 3D car models. For the 3D car models we select a subset of 50 car models from the popular ShapeNet dataset [2], which are rendered onto the background images at different elevations, distances and orientations.

The scenes are rendered using an equirectangular projection to images of dimension 512×256, covering a complete $360°$ field of view around the camera. Each rendered scene contains between one to three cars, which may be partially occluded. Object bounding boxes are automatically extracted and represented by the lat/lon coordinates (ϕ_i, θ_i) of the object's tangent plane as well as the object width w and height h on the tangent plane and its in-plane rotation α. All groundtruth coordinates are normalized to a range of $[-1.0, 1.0]$. In total, the dataset comprises $1,000$ test and $5,000$ training images with multiple objects each, out of which a subset of $1,000$ images is used as validation set.

For this task, we integrate the nearest neighbor variant (NN) of SphereNet into the Sphere-SSD framework (see Section 3.4) as it strikes a balance between computational efficiency and ease of integration into an object detection model. Because the graph and spherical convolution baselines are not applicable to the object detection task, we compare the performance of SphereNet to a CNN operating on the cube map (CubeMapCNN) and equirectangular representation (EquirectCNN). The latter is again tested in combination with a Spherical Transformer Network (EquirectCNN+SphereTN).

Following [30] we evaluate a version of EquirectCNN where the size of the convolutional kernels is enlarged towards the poles to approximate the object distortion in equirectangular images (EquirectCNN++). Like [30] we limit the maximum kernel dimension to 7×7. However, unlike [30] we keep weight tying in place for image rows with filters of the same dimension, thus reducing the number of model parameters. We thereby enable regular training of the network without kernel-wise knowledge distillation as in [30]. In addition, we utilize pre-trained weights when kernel dimensions match with the kernels in a pre-trained network architecture so that not all model parameters need to be trained from scratch.

As feature extractor all models use a VGG-16 network [26], which is initialized with weights pre-trained on the ILSVRC-2012-CLS dataset [23]. We change the max-pooling kernels to size 3×3 and use ReLU activations, L_2 regularization with weight $4e^{-5}$ and batch normalization in all layers of the network. Additional convolutional box prediction layers of depth $256, 128, 128, 128$ are attached to layer *conv5_3*. Anchors of scale 0.2 to 0.95 are generated for layer *conv4_3*, *conv5_3* and the box prediction layers. The aspect ratio for all anchor boxes is fixed to the aspect ratio of the side view of the rendered cars $(2 : 1)$. The full network is trained end-to-end in the Sphere-SSD framework with the RMSProp optimizer, batches of size 5 and a learning rate of 0.004.

Results on FlyingCars: Table 2 presents the results for the object detection task on the FlyingCars dataset after $50,000$ steps of training. Following common practice, we use an intersection-over-union (IoU) threshold of 0.5 for evaluation. Again, our results demonstrate that SphereNet outperforms the baseline methods. Qualitative results of the SphereNet model are shown in Fig. 6.

Compared to the classification experiments, the Spherical Transformer Network (SphereTN) demonstrates less competitive performance as no transformation is able to account for undistorting all objects in the image at the same time. It is thus outperformed by the EquirectCNN. The performance of the EquirectCNN model is improved when the kernel size is enlarged towards the poles (EquirectCNN++), but all EquirectCNN models perform worse than the CNN operating on a cube map representation (CubeMapCNN). The reason for the improved performance of the CubeMapCNN compared to the classification task is most likely that discontinuities at the patch boundaries are less often present in the FlyingCars dataset due to the smaller relative size of the objects.

Besides accuracy, another important property of an object detector is its training and inference speed. Table 2 therefore additionally lists the training time per batch and inference time per image on an NVIDIA Tesla K20. The numbers show similar runtimes for EquirectCNN and CubeMapCNN. SphereNet has a small runtime overhead of factor 1.1 to 1.2, while the EquirectCNN++ and EquirectCNN+SphereTN models have a larger runtime overhead of factor 1.8 for training and 1.9 to 2.5 for inference.

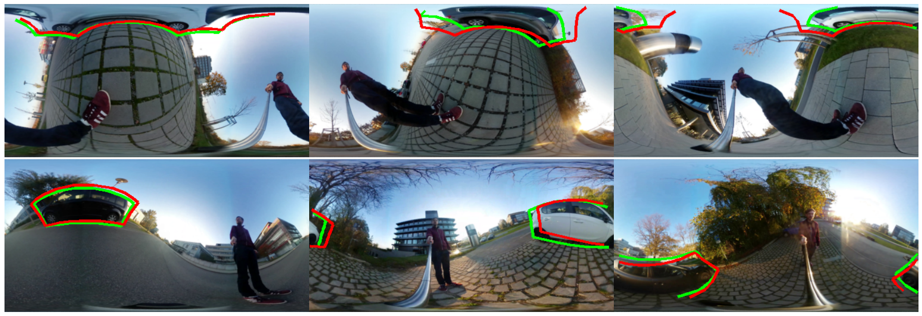

Fig. 7: **Detection Results on OmPaCa Dataset.** The ground truth is shown in green, our SphereNet (NN) results in red.

Table 3: **Transfer Learning Results on OmPaCa Dataset.** We transfer detection models trained on perspective images from the KITTI dataset [7] to an omnidirectional representation and finetune the models on the OmPaCa dataset.

Method	Test mAP (%)
CubeMapCNN	34.19
EquirectCNN	43.43
SphereNet (NN)	**49.73**

4.3 Transfer Learning: OmPaCa

Finally, we consider the transfer learning task, where a model trained on a perspective dataset is transferred to handle omnidirectional imagery. For this task we record a new real-world dataset of omnidirectional images of real cars with a handheld action camera. The images are recorded at different heights and orientations. The *omnidirectional parked cars (OmPaCa)* dataset consists of $1,200$ labeled images of size 512×256 with more than 50 different car models in total. The dataset is split into 200 test and $1,000$ training instances, out of which a subset of 200 is used for validation.

We use the same detection architecture and training parameters as in Section 4.2 but now start from a perspective SSD model trained on the KITTI dataset [7], convert it to our Sphere-SSD framework and fine-tune for $20,000$ iterations on the OmPaCa dataset. For this experiment we only compare against the EquirectCNN and CubeMapCNN baselines. Both the EquirectCNN+SphereTN as well as the EquirectCNN++ are not well suited for the transfer learning task due to the introduction of new model parameters, which are not present in the perspective detection model and which would thus require training from scratch.

Results on OmPaCa: Our results for the transfer learning task on the OmPaCa dataset are shown in Table 3 and demonstrate that SphereNet outperforms both baselines. Unlike in the object detection experiments on the FlyingCars dataset, the CubeMapCNN performs worse than the EquirectCNN by a large margin of nearly 10%, indicating that the cube map representation is not well suited for the transfer of perspective models to omnidirectional images. On the other hand, SphereNet performs better than the EquirectCNN by more than 5%, which confirms that the SphereNet approach is better suited for transferring perspective models to the omnidirectional case.

A selection of qualitative results for the SphereNet model is visualized in Fig. 7. As evidenced by our experiments, the SphereNet model is able to detect cars at different elevations on the sphere including the polar regions where regular convolutional object detectors fail due to the heavy distortions present in the input images. Several additional qualitative comparisons between SphereNet and the EquirectCNN model for objects located in the polar regions are provided in the supplementary material.

5 Conclusion and Future Work

We presented SphereNet, a framework for deep learning with 360° cameras. SphereNet lifts 2D convolutional neural networks to the surface of the unit sphere. By applying 2D convolution and pooling filters directly on the sphere's surface, our model effectively encodes distortion invariance into the filters of convolutional neural networks. Wrapping the convolutional filters around the sphere further avoids discontinuities at the borders or poles of the equirectangular projection. By updating the sampling locations of the convolutional filters we allow for easily transferring perspective CNN models to handle omnidirectional inputs. Our experiments show that the proposed method improves upon a variety of strong baselines in both omnidirectional image classification and object detection.

We expect that with the increasing availability and popularity of omnidirectional sensors in both the consumer market (e.g., action cameras) as well as in industry (e.g., autonomous cars, virtual reality), the demand for specialized models for omnidirectional images such as SphereNet will increase in the near future. We therefore plan to exploit the flexibility of our framework by applying it to other related computer vision tasks, including semantic (instance) segmentation, optical flow and scene flow estimation, single image depth prediction and multi-view 3D reconstruction in the future.

References

1. Bruna, J., Mallat, S.: Invariant scattering convolution networks. IEEE Trans. on Pattern Analysis and Machine Intelligence (PAMI) **35**(8), 1872–1886 (2013) 4
2. Chang, A.X., Funkhouser, T.A., Guibas, L.J., Hanrahan, P., Huang, Q., Li, Z., Savarese, S., Savva, M., Song, S., Su, H., Xiao, J., Yi, L., Yu, F.: Shapenet: An information-rich 3d model repository. arXiv.org **1512.03012** (2015) 11
3. Cohen, T.S., Geiger, M., Köhler, J., Welling, M.: Spherical CNNs. In: International Conference on Learning Representations (2018) 3, 9, 10
4. Cohen, T.S., Welling, M.: Group equivariant convolutional networks. In: Proc. of the International Conf. on Machine learning (ICML) (2016) 2, 4
5. Dai, J., Qi, H., Xiong, Y., Li, Y., Zhang, G., Hu, H., Wei, Y.: Deformable convolutional networks. Proc. of the IEEE International Conf. on Computer Vision (ICCV) **1703.06211** (2017) 4

6. Defferrard, M., Bresson, X., Vandergheynst, P.: Convolutional neural networks on graphs with fast localized spectral filtering. In: Advances in Neural Information Processing Systems (NIPS) (2016) 9
7. Geiger, A., Lenz, P., Urtasun, R.: Are we ready for autonomous driving? The KITTI vision benchmark suite. In: Proc. IEEE Conf. on Computer Vision and Pattern Recognition (CVPR) (2012) 13
8. He, K., Zhang, X., Ren, S., Sun, J.: Deep residual learning for image recognition. In: Proc. IEEE Conf. on Computer Vision and Pattern Recognition (CVPR) (2016) 4
9. Henriques, J.F., Vedaldi, A.: Warped convolutions: Efficient invariance to spatial transformations. In: Proc. of the International Conf. on Machine learning (ICML) (2017) 4
10. Hu, H.N., Lin, Y.C., Liu, M.Y., Cheng, H.T., Chang, Y.J., Sun, M.: Deep 360 pilot: Learning a deep agent for piloting through 360° sports video. In: Proc. IEEE Conf. on Computer Vision and Pattern Recognition (CVPR) (2017) 1
11. Jaderberg, M., Simonyan, K., Zisserman, A., Kavukcuoglu, K.: Spatial transformer networks. In: Advances in Neural Information Processing Systems (NIPS) (2015) 4
12. Jeon, Y., Kim, J.: Active convolution: Learning the shape of convolution for image classification. In: Proc. IEEE Conf. on Computer Vision and Pattern Recognition (CVPR) (2017) 4
13. Jia, Y.: Learning Semantic Image Representations at a Large Scale. Ph.D. thesis, EECS Department, University of California, Berkeley (May 2014), http://www2.eecs.berkeley.edu/Pubs/TechRpts/2014/EECS-2014-93.html 7
14. Khasanova, R., Frossard, P.: Graph-based classification of omnidirectional images. In: Proc. of the IEEE International Conf. on Computer Vision (ICCV) Workshops (2017) 3, 9, 10
15. Khasanova, R., Frossard, P.: Graph-based isometry invariant representation learning. In: Proc. of the International Conf. on Machine learning (ICML) (2017) 3
16. Lai, W., Huang, Y., Joshi, N., Buehler, C., Yang, M., Kang, S.B.: Semantic-driven generation of hyperlapse from 360 degree video (2017) 1
17. Liu, W., Anguelov, D., Erhan, D., Szegedy, C., Reed, S.E., Fu, C., Berg, A.C.: SSD: single shot multibox detector. In: Proc. of the European Conf. on Computer Vision (ECCV) (2016) 8
18. Ma, J., Wang, W., Wang, L.: Irregular convolutional neural networks (2017) 4
19. Monroy, R., Lutz, S., Chalasani, T., Smolic, A.: Salnet360: Saliency maps for omnidirectional images with cnn. In: ICME (2017) 3
20. Pearson, F.: Map Projections: Theory and Applications. Taylor & Francis (1990) 4, 5
21. Ran, L., Zhang, Y., Zhang, Q., Yang, T.: Convolutional neural network-based robot navigation using uncalibrated spherical images. Sensors **17**(6) (2017) 1
22. Ruder, M., Dosovitskiy, A., Brox, T.: Artistic style transfer for videos and spherical images. arXiv.org **abs/1708.04538** (2017) 3
23. Russakovsky, O., Deng, J., Su, H., Krause, J., Satheesh, S., Ma, S., Huang, Z., Karpathy, A., Khosla, A., Bernstein, M., Berg, A.C., Fei-Fei, L.: Imagenet large scale visual recognition challenge. International Journal of Computer Vision (IJCV) (2015) 12
24. Saff, E.B., Kuijlaars, A.B.J.: Distributing many points on a sphere. The Mathematical Intelligencer **19**(1), 5–11 (1997) 7, 8
25. Sifre, L., Mallat, S.: Rotation, scaling and deformation invariant scattering for texture discrimination. In: Proc. IEEE Conf. on Computer Vision and Pattern Recognition (CVPR) (2013) 4
26. Simonyan, K., Zisserman, A.: Very deep convolutional networks for large-scale image recognition. In: Proc. of the International Conf. on Learning Representations (ICLR) (2015) 4, 12
27. Su, Y.C., Grauman, K.: Making 360deg video watchable in 2d: Learning videography for click free viewing. In: Proc. IEEE Conf. on Computer Vision and Pattern Recognition (CVPR) (2017) 1

28. Su, Y.C., Jayaraman, D., Grauman, K.: Pano2vid: Automatic cinematography for watching 360 degree videos. In: Proc. of the Asian Conf. on Computer Vision (ACCV) (2016) 1
29. Worrall, D.E., Garbin, S.J., Turmukhambetov, D., Brostow, G.J.: Harmonic networks: Deep translation and rotation equivariance. In: Proc. IEEE Conf. on Computer Vision and Pattern Recognition (CVPR) (2017) 2, 4
30. Yu-Chuan Su, K.G.: Flat2sphere: Learning spherical convolution for fast features from 360° imagery. In: Advances in Neural Information Processing Systems (NIPS) (2017) 3, 12
31. Zhou, Y., Ye, Q., Qiu, Q., Jiao, J.: Oriented response networks. In: Proc. IEEE Conf. on Computer Vision and Pattern Recognition (CVPR) (2017) 4